Title
Enhanced Predictability of Eastern North Pacific Tropical Cyclone Activity Using the ENSO Longitude Index

Journal
Geophysical Research Letters, 47(16)

ISSN
0094-8276

Authors
Balaguru, Karthik
Patricola, Christina M
Hagos, Samson M
et al.

Publication Date
2020-08-28

DOI
10.1029/2020gl088849

Peer reviewed

Enhanced predictability of Eastern Pacific Hurricane activity using the ENSO Longitude Index

Karthik Balaguru[1], Christina M. Patricola[2,3], Samson M. Hagos[1], L. Ruby Leung [1], and Lu Dong[1]

[1]Pacific Northwest National Laboratory, Richland, WA, USA
[2]Lawrence Berkeley National Laboratory, Berkeley, CA, USA
[3]Iowa State University, Ames, IA, USA

Key Points:

- The ENSO Longitude Index (ELI) can be used to predict Eastern Pacific hurricane activity with a lead time of 6 months.
- ELI outperforms traditional ENSO indices because it better captures changes in upper-ocean thermal structure associated with ENSO.
- These results have substantial implications for operational seasonal forecasts of Eastern Pacific hurricanes.

Corresponding author: Karthik Balaguru, `Karthik.Balaguru@pnnl.gov`

Abstract

Past studies have indicated that El Niño-Southern Oscillation (ENSO) plays a major role in the interannual variability of Eastern Pacific hurricane activity. The primary mechanism being the eastward displacement of the warm pool during an El Niño, which carries warm water into that basin thereby creating favorable oceanic conditions. Despite this, the question of whether an accurate knowledge of ENSO enhances seasonal predictability of Eastern Pacific hurricanes has not been addressed specifically. In this study, we show that unlike traditional indices of ENSO, the ENSO Longitude Index (ELI) is able to predict Eastern Pacific hurricane activity at significant lead times. By capturing changes in the location of deep convection and associated thermocline processes more accurately, ELI explains the most variability in the upper-ocean heat content in the Eastern Pacific basin compared to other ENSO indices. These results have substantial implications for operational seasonal forecasts of Eastern Pacific hurricanes.

Plain Language Summary

During an El Niño, the warm water that traditionally resides in the tropical western Pacific migrates to the eastern part of the basin, causing an increase in the upper-ocean heat content and thereby enhances hurricane activity in the Eastern Pacific. This is because heat energy available at the ocean surface is extracted by storms passing over them and used as fuel for their intensification. Despite this knowledge, the question of whether an accurate information of El Niño-Southern Oscillation (ENSO) improves seasonal predictability of Eastern Pacific hurricanes remains unanswered to date. In this study, we show that unlike traditional indices of ENSO that are based on fixed thresholds and are almost empirical, the ENSO Longitude Index (ELI) improves the predictability of Eastern Pacific hurricanes significantly at lead times of 5-6 months facilitated by the ocean's memory. By accounting for changes in the Walker Circulation, and associated east-west shifts in the location of deep convection and warm water volume, ELI better explains interannual variations in the upper-ocean heat content in the Eastern Pacific hurricane basin. These results promote the use of ELI for operational seasonal forecasts of Eastern Pacific hurricane activity.

1 Introduction

The Eastern Pacific hurricane basin is the second most active among all the tropical cyclone basins in the world (Gray & Brody, 1967). When considering hurricanes of all categories including tropical storm strength, nearly 20% have made landfall over the Mexican coast during the period 1951-2000 (Jáuregui, 2003; Blake, 2009). On average, there is at least one storm producing hurricane-force winds along the Pacific coast each year causing substantial damages to life and property (Blake, 2009). For instance, Hurricane Manuel during the 2013 season caused widespread floods upon landfall resulting in mud slides and considerable loss of life (T. B. Kimberlain, 2014). In October 2015, Hurricane Patricia underwent explosive intensification before becoming the strongest hurricane on record in the Western Hemisphere and caused substantial damages upon landfall (Rogers et al., 2017; Foltz & Balaguru, 2016). Although less frequent, Eastern Pacific hurricanes are also known to affect the Hawaiian islands from time to time (Chiu, 1983; Coffman & Noy, 2012). Finally, the moisture from some of these hurricanes is shown to cause substantial rainfall in the southwest United States and contribute majorly to the water budget of that region (Corbosiero et al., 2009; Ritchie et al., 2011). Considering the above, it becomes very important to improve our knowledge of the factors affecting Eastern Pacific hurricanes.

On subseasonal timescales, the formation of hurricanes in the Eastern Pacific is modulated by the Madden-Julian Oscillation through zonal wind anomalies associated with the equatorial Kelvin wave propagation (Maloney & Hartmann, 2000; Camargo et al., 2008; Boucharel, Jin, England, et al., 2016; Camargo et al., 2019). At interannual timescales however, El Niño-Southern Oscillation (ENSO) exerts the dominant control over global climate variability (McPhaden, 1999), including in the tropical Eastern Pacific region (Wang & Fiedler, 2006). Considering this, several studies have attempted to understand the ENSO effects on Eastern Pacific hurricanes (Chu, 2004). During the warm El Niño phase, hurricane activity in this basin is found to increase with storms getting stronger and lasting longer (Chu, 2004). El Niño's influence on Eastern Pacific hurricanes depends on the spatial pattern of SST warming, or ENSO diversity (Patricola et al., 2016; Boucharel, Jin, Lin, et al., 2016). While changes in the largescale environment favorable for hurricanes during an El Niño were noted in the Central Pacific region (Chu, 2004; Collins et al., 2016; Klotzbach & Blake, 2013), the response was less clear in the Eastern Pacific (Whitney & Hobgood, 1997). This was confirmed by a later study that showed that the influence of the environment on hurricane activity was more readily seen in the region to the west of 116°W when compared to the region to its east (Collins & Mason, 2000), which has been attributed to a modulation of ENSO's influence on TCs by the Central American Gap Winds (Fu et al., 2017). However, these studies primarily considered atmospheric factors and sea surface temperatures (SSTs).

During an El Niño, the trade winds over the equatorial Pacific weaken and, consequently, the warm pool and the location of deep convection in the western Pacific begin migrating eastwards (Kessler & McPhaden, 1995; McPhaden & Yu, 1999). Associated with this phenomenon, downwelling equatorial Kelvin waves are generated that transport the signal in the thermocline to the central and eastern equatorial Pacific. After impinging the eastern boundary, the planetary waves bifurcate into coastal Kelvin waves that further propagate the signal north and south. At interannual timescales, variations in thermocline associated with ENSO are primarily responsible for those in upper-ocean heat content in the Eastern Pacific basin, especially in the region to the south of 20°N that includes the hurricane main development region (Balaguru et al., 2013). Further, the timescale for oceanic adjustment to the ENSO atmospheric forcing is such that thermocline and oceanic heat content anomalies in the Eastern Pacific appear approximately 6 months after the peak of equatorial Pacific SST anomalies during boreal winter (Jin et al., 2014). Based on this, it was suggested that an accurate knowledge of ENSO may improve seasonal forecasts of Eastern Pacific hurricanes (Jin et al., 2014). However, such an evaluation has not been performed to date. In this study, we examine the ability of various ENSO indices to predict seasonal hurricane activity in the Eastern Pacific basin at 6 month lead times and explain the differences based on the large-scale ocean-atmosphere conditions.

2 Methods

2.1 Data

Eastern Pacific hurricane track data (HURDAT2) (Landsea & Franklin, 2013) for the 40-year period 1979-2018, obtained from the National Hurricane Center (NHC) at `https://www.nhc.noaa.gov/data/`, are used to estimate hurricane Power Dissipation Index (PDI) and frequency, and to identify the locations of Rapid Intensification. Monthly mean atmospheric temperature, humidity, sea-level pressure, horizontal winds and SST, based on the European Centre for Medium-Range Weather Forecasts (ECMWF) atmospheric reanalysis (ERA5) (Hersbach & Dee, 2016), are obtained from `https://www.ecmwf.int/en/forecasts/datasets/reanalysis-datasets/era5` for the period 1979-2018. These data are used to estimate the hurricane Ventilation Index (VI) and the column moisture deficit. Monthly mean vertical ocean temperature profiles based on the National Centers for Environmental Prediction (NCEP) Global Ocean Data Assimilation System (GODAS) (Behringer & Xue, 2004), obtained from `https://www.cpc.ncep.noaa.gov/products/GODAS/` for the period 1980-2018, are used to estimate the Dynamic Temperature (Tdy) and the Tropical Cyclone Heat Potential (TCHP). Maps of the monthly mean sea surface height (SSH) relative to the geoid, also obtained from NCEP-GODAS, are used to understand the response of the upper-ocean to ENSO forcing.

To validate our results based on ERA5, we also computed the VI using atmospheric data based on NCEP2 reanalysis (Kanamitsu et al., 2002), available at `https://www.esrl.noaa.gov/psd/data/gridded/data.ncep.reanalysis2.html`, and SST from the UK Met Office Hadley Centre (Rayner et al., 2003), available at `https://www.metoffice.gov.uk/hadobs/hadisst/`. To support our results based on NCEP-GODAS, we also computed Tdy from ocean temperature profiles based on the ECMWF Ocean Reanalysis System (ORAS4) (Balmaseda et al., 2013). These data are available for download from `http://icdc.cen.uni-hamburg.de`. Various ENSO indices are obtained and used to evaluate the predictability of Eastern Pacific hurricane activity. We use four different indices: 1) Oceanic Niño Index (ONI) (Trenberth, 1997), available from `http://origin.cpc.ncep.noaa.gov/products/analysis_monitoring/ensostuff/ONI_v5.php`, 2) Southern Oscillation Index (SOI) (Kiladis & van Loon, 1988), available from `https://www.cpc.ncep.noaa.gov/data/indices/soi`, 3) Multivariate ENSO Index (MEI) (Wolter & Timlin, 2011), available from `https://www.esrl.noaa.gov/psd/enso/mei/`, and 4) ENSO Longitude Index (ELI) (Williams & Patricola, 2018), available from `https://portal.nersc.gov/archive/home/projects/cascade/www/ELI`. Data for wildfire occurrence, obtained from `https://www.mtbs.gov/direct-download`, are used to correlate frequency of wildfires with hurricane activity.

2.2 Calculations

Traditional ENSO indices such as ONI are defined as an SST anomaly in a fixed region. However, such indices fail to capture the diversity of ENSO events (i.e., variations in the spatial patterns of SST warming) that are important in shaping teleconnections with extremes. In contrast, the ENSO Longitude Index (ELI) represents the average longitude of deep convection in the equatorial Pacific, and therefore characterizes ENSO-driven zonal shifts in the location of deep convection in the Walker Circulation. ELI captures the diversity and extremes of ENSO and recovers the familiar global responses in precipitation and temperature. ELI is calculated using only monthly SST as input, and is the average of all longitudes in equatorial Pacific over which SST meets or exceeds the convective threshold, which is approximated as the tropical-average SST over 5°S-5°N (Williams & Patricola, 2018).

To understand the role of the largescale environment in hurricane activity, we employ the VI, which is a combination of dynamic and thermodynamic parameters that play a critical role in hurricane intensification. Following Tang and Emanuel (2012), the VI is computed as follows

$$VI = \frac{\chi_m . U_{shear}}{U_{PI}} \tag{1}$$

where χ_m represents the entropy deficit in the mid-troposphere, u_{shear} is the vertical wind shear and u_{PI} is the Potential Intensity. The entropy deficit term(χ_m) is calculated as

$$\chi_m = \frac{{S_m}^* - S_m}{{S_{SST}}^* - S_b} \tag{2}$$

Here, ${S_m}^*$ and S_m are the saturation moist entropy and the moist entropy respectively in the mid-troposphere (evaluated at 600 hPa), ${S_{SST}}^*$ is saturation moist entropy at the sea surface and S_b is the moist entropy in the boundary layer above it (evaluated at 925 hPa). Physically, χ_m represents the loss of entropy in the mid-troposphere through dry air intrusion normalized by entropy gain at the air-sea interface through enthalpy fluxes. The pseudoadiabatic moist entropy is calculated using the approximate formula provided in Bryan (2008).

The vertical wind shear (U_{shear}) is estimated as the magnitude of the vector difference between horizontal winds at the 200 and 850 hPa levels (DeMaria, 1996). U_{PI} represents the theoretical maximum intensity that a hurricane can attain under the prevailing environmental conditions (K. A. Emanuel, 1999). It is calculated as

$$U_{PI} = \sqrt{\frac{C_k}{C_d}\frac{SST - T_o}{T_o}(K_s - K_b)} \tag{3}$$

Here, C_k and C_d are the coefficients of enthalpy and drag respectively, T_o is the outflow temperature, K_s and K_b are the saturation specific enthalpy at the sea surface and in the ambient boundary layer respectively. The program to compute U_{PI} is available at `ftp://texmex.mit.edu/pub/emanuel/TCMAX/`. In general, low values for U_{shear} and χ_m, and high values for U_{PI} favor hurricane development. Hence, when the VI is low (high), the largescale environment is more (less) conducive for hurricane formation and intensification.

To evaluate the role of the ocean subsurface in hurricane intensification, we compute the Tdy (Balaguru et al., 2015). Unlike the pre-storm SST, the Tdy accounts for the effects of upper-ocean stratification on hurricane-induced vertical mixing and sea surface cooling, and hence represents the true SST felt by the core of the storm (Balaguru et al., 2015). We first estimate the hurricane mixing length (L) as follows

$$L = h + (\frac{\rho_o.{u_*}^3.t}{\kappa.g.\alpha})^{\frac{1}{3}} \tag{4}$$

Here, h is the initial mixed layer depth, ρ_o is the density of seawater, u_* is the friction velocity, t is the time period of mixing, κ is the Von Kármán constant, g is the acceleration due to gravity, and α is the upper-ocean stratification or the rate of change of density beneath the mixed layer. To isolate the effect of the ocean, we compute Tdy with a fixed storm state where the surface wind speed is set at 50 ms^{-1}, the translation speed is a typical 5 ms^{-1} and a radius of maximum winds of 50 km. For further details regarding the calculation of L, see Balaguru et al. (2015). Having computed L, we then calculate Tdy as the temperature averaged over the depth of L as

$$Tdy = \frac{1}{L}\int_0^L T(z)dz \tag{5}$$

To support our results based on Tdy, we also compute TCHP, defined as the integral of the temperature from the surface to the depth of the 26^{o}C isotherm (Shay & Brewster, 2010).

$$TCHP = \int_0^{z26} \rho C_p(T(z) - 26)dz \tag{6}$$

Here, T(z) is the temperature (T) as a function of depth (z). The atmospheric column moisture deficit is calculated as

$$Moisture\ deficit = 1 - (\frac{\int qdp}{\int q_s dp}) \tag{7}$$

Here, q is the specific humidity and q_s is the saturation specific humidity. For each season, the hurricane Power Dissipation Index (PDI) is estimated as the sum of cube of wind speeds at each 6-hourly location along tracks, integrated over all storms for that season (K. Emanuel, 2005). Empirical Orthogonal Function (EOF) analysis was carried out using the 'eofs' python package (Dawson, 2016).

3 Results

We begin by examining the track density of Eastern Pacific hurricanes based on 40-years of best track data (Fig. 1A). Despite being the second most active basin in the world (Gray & Brody, 1967), the majority of the tracks are confined to a narrow band and the largest values of track density are found in the region: 130°W-100°W, 10°N-22°N (black box in Fig. 1A). The composite mean seasonal cycle of the PDI for the Eastern Pacific is shown in Fig. 1B. When compared to the Atlantic, the climatological peak of Eastern Pacific hurricane activity is broader and ranges from July-October (`https://www.nhc.noaa.gov/climo/`). Averaged over these months, the mean PDI is about 1.97E7 kt^3. Next, we consider the composite mean seasonal cycle of PDI for El Niño years, identified as those years where the previous December-February averaged ELI exceeds 161, i.e., the location of deep convection has migrated to the east of 161°E longitude. Based on this, ten years have been identified as El Niño years during the 40-year period 1979-2018: 1983, 1987, 1991, 1992, 1993, 1995, 1998, 2003, 2010 and 2016. The composite mean PDI for these years indicates that during the summer following an El Niño, hurricane activity in this basin tends to be more active, consistent with previous studies (Gray & Sheaffer, 1991; Chu, 2004; Romero-Vadillo et al., 2007; Camargo et al., 2008; Balaguru et al., 2013; Jin et al., 2014; Caron et al., 2015). The July-October averaged PDI increases by more than 25% to 2.53E7 kt^3. What causes this increase in hurricane activity during the summer following an El Niño?

To address this, we consider the largescale ambient environment using the VI, a combination of critical dynamic and thermodynamic parameters that govern hurricane development (Fig. 1C). The climatological seasonal cycle of VI, averaged over the box shown in Fig. 1A, is in good agreement with the seasonal cycle of hurricane activity. The lowest values of VI are found during the months of July-October, coinciding with the peak of the hurricane season. However, when we consider the composite mean seasonal cycle of VI for the summers following an El Niño, we find that the values are similar or slightly larger, suggesting that the largescale atmospheric environment is less conducive for hurricanes, as has been noted previously (Boucharel, Jin, Lin, et al., 2016). Averaged over the months of July-October, the VI increases by about 10% when compared to climatology. Thus, atmospheric factors are unable to explain the increase in hurricane activity associated with an El Niño in this basin. Similar conclusions were reached in a few previous studies that couldn't establish a link between changes in environmental parameters and hurricane activity associated with ENSO in this basin (Whitney & Hobgood, 1997; Collins & Mason, 2000; Jien et al., 2015). So how can we explain the ENSO effect on Eastern Pacific hurricanes?

In the Northern Hemisphere, the upper-ocean heat content has been shown to play a significantly larger role in the intensification of Eastern Pacific hurricanes when compared to other basins (Balaguru et al., 2015). Hence, we next examine the climatological mean seasonal cycle of Tdy, a metric for the ocean heat content relevant for hurricanes (Fig. 1D). Again, the seasonal cycle of Tdy, averaged over the box shown in Fig. 1A, is consistent with that of hurricane activity with maximum values occurring from July-September. Unlike VI however, the Tdy during the summer following an El Niño is more conducive for hurricane intensification. Averaged over the months of July-October, the Tdy is 24.40°C whereas the climatological mean is 24.18°C. This increase of 0.22°C is significantly higher than the standard error, which is about 0.1°C, and hence is statistically significant. Therefore, larger values of Tdy, which indicate an increase in the upper-ocean heat content, is likely the primary mechanism through which an El Niño fuels an increase in Eastern Pacific hurricane activity (Balaguru et al., 2013; Jin et al., 2014).

To further understand the role of upper-ocean heat content in Eastern Pacific hurricanes, we explore the spatial pattern of Tdy variability and its relationship with hurricane activity in this basin. The first EOF of July-October averaged Tdy, expressed as the correlation between the leading principal component (PC) time series and the time series of Tdy at each grid point, is shown in Fig. 1E. Nearly 40% of interannual variability is explained by this leading mode. Maximum values are found along the Central American coast, between 110°W and 90°W, and gradually decrease westwards into the basin. The region with high Tdy variability near the coast coincides very well with the region of highest hurricane track densities (Fig. 1A), indicating that the leading mode may be tightly related to hurricane activity in this basin. To substantiate this, consider the map of correlation between the timeseries of PDI and July-October averaged Tdy (Fig. 1F). The spatial pattern of correlation coefficients is in good agreement with that of the first EOF of Tdy (Fig. 1E), underlining the influence of Tdy on hurricanes in this basin. Again, highest correlations are found along the coast and decrease westwards into the interior of the basin. Finally, the correlation between the PC timeseries of the leading EOF and the PDI is 0.61, suggesting that the former explains about 37% of the variance in hurricane activity. These results firmly establish the significance of upper-ocean heat content for Eastern Pacific hurricanes.

Since interannual variations in upper-ocean heat content in this basin are linked to ENSO through planetary wave propagation (Jin, 1996; McPhaden, 1999; Jin et al., 2014), the above results naturally lead us to the following question: Can an accurate knowledge of ENSO conditions possibly help enhance seasonal forecasts of Eastern Pacific hurricanes? To address this, we computed the correlation between the December-February averaged ENSO index and the PDI for the following summer over the 40-year period 1979-2018 (Table 1). Four different ENSO indices are used: 1) Ocean-based ONI, 2) Atmosphere-based SOI, 3) Air-sea coupled MEI, and 4) ELI. The correlation between ONI and PDI is 0.16 and is not statistically significant. The correlation coefficients for PDI with SOI and MEI are -0.23 and 0.2 respectively, and hence the variance explained ranges from 4-5 % approximately. On the other hand, the PDI correlates with ELI at 0.28, indicating a significantly higher variance explained of nearly 8% (Table 1). While these are results when considering the entire Eastern Pacific basin (east of 140°W), the differences are even more significant when we consider the eastern part of the basin where previous studies struggled (Whitney & Hobgood, 1997; Collins & Mason, 2000). In the region to the east of 115°W, the correlation between PDI and various ENSO indices are: 0.17 for ONI, -0.24 for SOI, 0.23 for MEI and 0.34 for ELI. Thus the variance explained for ONI, SOI and MEI range between 3% and 6%. On the other hand, the variance explained for ELI almost doubles to 11% (Table 1).

The calculation of PDI is heavily influenced by the presence of major hurricanes. Also, the damage inflicted by major hurricanes is disproportionately high when compared to weaker storms (K. Emanuel, 2005). Hence, we next consider the predictability of the frequency of major hurricanes. The correlations for the frequency of major hurricanes with ONI (0.15), SOI (-0.19) and MEI (0.19) are statistically insignificant. However, the major hurricane frequency correlates with ELI at 0.26 and is significant at the 90% level (Table 1). As for PDI, the superiority of ELI over other indices increases when we consider the region to the east of 115°W. The correlation with the frequency of major hurricanes for ONI, MEI and SOI are 0.1,-0.17 and 0.15 respectively, which are not statistically significant. But with ELI, the correlation for major hurricane frequency is 0.25 and is significant at the 90% level.

One other aspect of hurricane intensification that is extremely challenging to forecast is the occurrence of rapid intensification, defined as an increase in intensity of 30 kt or higher in a day (Rappaport et al., 2009). For instance, Hurricane Patricia (2016), the strongest hurricane on record in the Western Hemisphere, intensified by more than 100 kt in 24 hrs before making landfall on the Mexican coast (Foltz & Balaguru, 2016).

The operational forecasts for the storm by the NHC severely underestimated its intensity by 60-100 kt (T. Kimberlain et al., 2016). Since upper-ocean heat content is one of the most important predictors of hurricane rapid intensification in the Eastern Pacific (Kaplan et al., 2015), we next consider the predictability of rapid intensification. The frequency of rapid intensification is not well-correlated with ONI, SOI and MEI (Table 1). However, the frequency of rapid intensification correlates with ELI at 0.22, a value significant at the 90% level. Even for the frequency of rapid intensification, the relative skill of ELI increases in the eastern part of the basin. The correlation coefficients for ONI, MEI and SOI are 0.14, -0.18 and 0.19 respectively and are not statistically significant. However, the correlation with ELI is about 0.3 and is significant at the 95% level. Thus, for all three metrics of hurricane activity, ELI outperforms other well-known ENSO indices indicating that ELI is able to predict Eastern Pacific hurricane activity with significant skill at a lead time of 5-6 months.

This brings us to the final question: How can we explain this enhanced efficiency of ELI? Previously, we have seen the important role played by variations in upper-ocean heat content (Tdy) in Eastern Pacific hurricanes. To understand the superiority of ELI, we correlate the PC timeseries of the leading EOF of July-October averaged Tdy with various ENSO indices: ONI, SOI and MEI correlate with the PC time series at 0.25, explaining 6% of the variance. On the other hand, ELI correlates with the PC timeseries at 0.32, increasing the variance explained to 10%. Similar results are obtained using TCHP (Table 1), another metric of the upper-ocean heat content (Shay & Brewster, 2010). This suggests that the enhanced skill of ELI with regards to predicting the interannual variability of Eastern Pacific hurricane activity is mainly related to its ability to explain interannual variations in upper-ocean heat content. The main characteristic feature of ELI that separates it from other ENSO indices is its ability to classify the diversity or 'flavor' of El Niño events (Williams & Patricola, 2018). While indices such as ONI are almost empirically based, the ELI accounts for the tropical convective threshold and is able to more accurately identify shifts in deep convection associated with ENSO (Williams & Patricola, 2018). Since different types of El Niño affect upper-ocean heat content differently, the ELI is more skillful than other ENSO indices at predicting hurricane activity at 6 month lead times.

To illustrate this, we consider the response of the tropical Pacific upper-ocean thermal structure to ENSO (Fig. 2). The climatological January-May averaged SSH, an indicator of the warm water volume in the upper layer of the ocean (Wyrtki, 1985), is shown in Fig. 2A. Higher values of SSH are found in the west and lower values in the east, signifying that much of the warm water is piled up in the western Pacific. This zonal contrast in sea-level is maintained in place by easterly winds at the surface, which represent the lower branch of the Walker Cell. The anomalous January-May averaged SSH following the 1997-98 El Niño, the strongest event based on ELI, is shown in Fig. 2B. The spatial pattern of SSH anomalies is consistent with the 'discharge' phase of the 'recharge-discharge' ENSO paradigm (Jin, 1997; Meinen & McPhaden, 2000). During this process, heat is transported away from the equator by Sverdrup transport induced by anomalous zonal westerly winds, resulting in negative anomalies along the equator and positive anomalies polewards of it (Jin, 1997; Meinen & McPhaden, 2000). Further, the warm water that has migrated to the eastern part of the basin is carried polewards by coastal Kelvin waves (Meinen & McPhaden, 2000). Note that the region with strong positive anomalies includes the Eastern Pacific hurricane basin (Fig. 1).

Compared to the 1997-98 El Niño, the SSH response following the 2015-16 El Niño (the strongest event based on ONI) is more muted (Fig. 2C). While the strongest positive SSH anomalies are closer to the eastern boundary for the 1997-98 El Niño (Fig. 2B), the maximum positive anomalies for the 2015-16 El Niño are found to the west of 100°W, and are considerably weaker. To understand this difference further, we examine the January-May averaged equatorial Pacific thermocline depth (Fig. 2D). The climatological thermocline, defined as the depth of the 20°C isotherm, is consistent with the climatological pattern of SSH. From a value of about 170 m near the date line, it decreases to 35 m at 80°W near the eastern boundary. Following the 1997-98 El Niño, the zonal gradient in the thermocline depth decreased considerably. The thermocline shoaled to a depth of about 125 m near the date line and deepened to a depth of 80 m near 80°W.

Although the zonal gradient in thermocline weakened following the 2015-16 El Niño also, the reduction was considerably smaller when compared to that following the 1997-98 El Niño. While the thermocline depth decreased to 145 m near the date line, it only increased to 40 m at 80°W. Thus, the thermocline change is particularly small near the eastern boundary, suggesting that the migration of the warm water to the easternmost part of the basin was significantly reduced during the 2015-16 El Niño. Thus, the zonal migration of the warm water in the equatorial Pacific is more in line with the El Niño as classified by ELI. This becomes clear when we consider the scatter between the slope of the equatorial Pacific thermocline and ELI (Fig. 2E). The slope of the thermocline varies almost linearly with ELI and the latter explains nearly 89% of its interannual variability. Though ONI is also well-correlated with the slope of the thermocline (Fig. 2F), the variance explained drops to 67%. The agreement between the slope of the thermocline and ONI is particularly poor for the strong El Niño events, as classified by ONI. Thus, through a more accurate estimation of the zonal migration of the location of deep convection and warm water near the eastern boundary, ELI better accounts for changes in upper-ocean heat content in the Eastern Pacific hurricane basin. While the results presented thus far are based on ERA5 atmospheric reanalysis and SST, and GODAS ocean reanalysis data, similar results are obtained using NCEP atmospheric reanalysis, Hadley SST and ORAS4 ocean reanalysis, (Figs. S1 and S2). Also, analysis of output from a high-resolution coupled model that can explicitly simulate hurricanes yields consistent results, highlighting the robustness of our main conclusions (Text S1, Fig. S3).

4 Summary and Discussion

In this study, we show that the predictability of Eastern Pacific hurricane activity is significantly enhanced when using the ENSO Longitude Index (ELI), which takes into account the prevailing threshold for deep convection in the tropics and hence more accurately identifies ENSO-related changes in the Walker Circulation and, consequently, the upper-ocean thermal structure. This holds true across three different metrics of hurricane activity including PDI, frequency of major hurricanes and the frequency of rapid intensification. This is primarily because the ELI is able to better predict variations in the upper-ocean heat content in the Eastern Pacific hurricane basin associated with different types of ENSO at a lead time of 6 months. Based on an EOF analysis of July-October mean Tdy, we find that the first EOF mode, which explains nearly a third of the variance in PDI, is more tightly correlated with ELI compared to other indices of ENSO. In light of this, we strongly advocate for the use of ELI for seasonal forecasts of Eastern Pacific hurricane activity.

Earlier, we had noted that the remnants of these storms contribute substantially to the annual rainfall in the southwest United States (Corbosiero et al., 2009; Ritchie et al., 2011). To support this idea, we computed the correlation between the column moisture deficit averaged over the region 118°W-104°W, 30°N-40°N and the hurricane PDI for the region 120°W-90°W, 10°N-20°N. For the 40-year period 1979-2018 and for the late season months of September-November, when hurricanes in this basin are likely to recurve (`https://www.nhc.noaa.gov/climo/`), the correlation is nearly -0.5. Thus, improving the seasonal forecasts of Eastern Pacific hurricanes could possibly improve that of precipitation for the arid regions in the southwestern United States. Late September through mid-November also tends to be the time when conditions in Southern California are the driest and the Santa Ana winds cause most wildfires (Rolinski et al., 2016). For the 34-year period 1984-2017 and for the months of September-November, a simple correlation between the number of wildfires in California and the PDI, computed over the same region, is about -0.28, a value significant at the 95% level. Thus, we speculate that Eastern Pacific hurricanes may also play a role in Californian wildfires through their impact on the environmental moisture. However, future studies are needed to examine this possibility in more detail.

While we have mainly focused on mechanisms operating at interannual timescales in this study, similar oceanic processes may also be at work at intraseasonal timescales (Boucharel, Jin, England, et al., 2016). Hence, the applicability of ELI at shorter timescales could also be potentially explored. Finally, while some studies indicate that extreme El Niño events are more likely to occur in future under global warming (Cai et al., 2014; Williams & Patricola, 2018), some others have pointed out the uncertainty associated with model projections of ENSO (Latif & Keenlyside, 2009). Our study suggests that a better understanding of the future of ENSO will likely lead to improved projections of future Eastern Pacific hurricane activity.

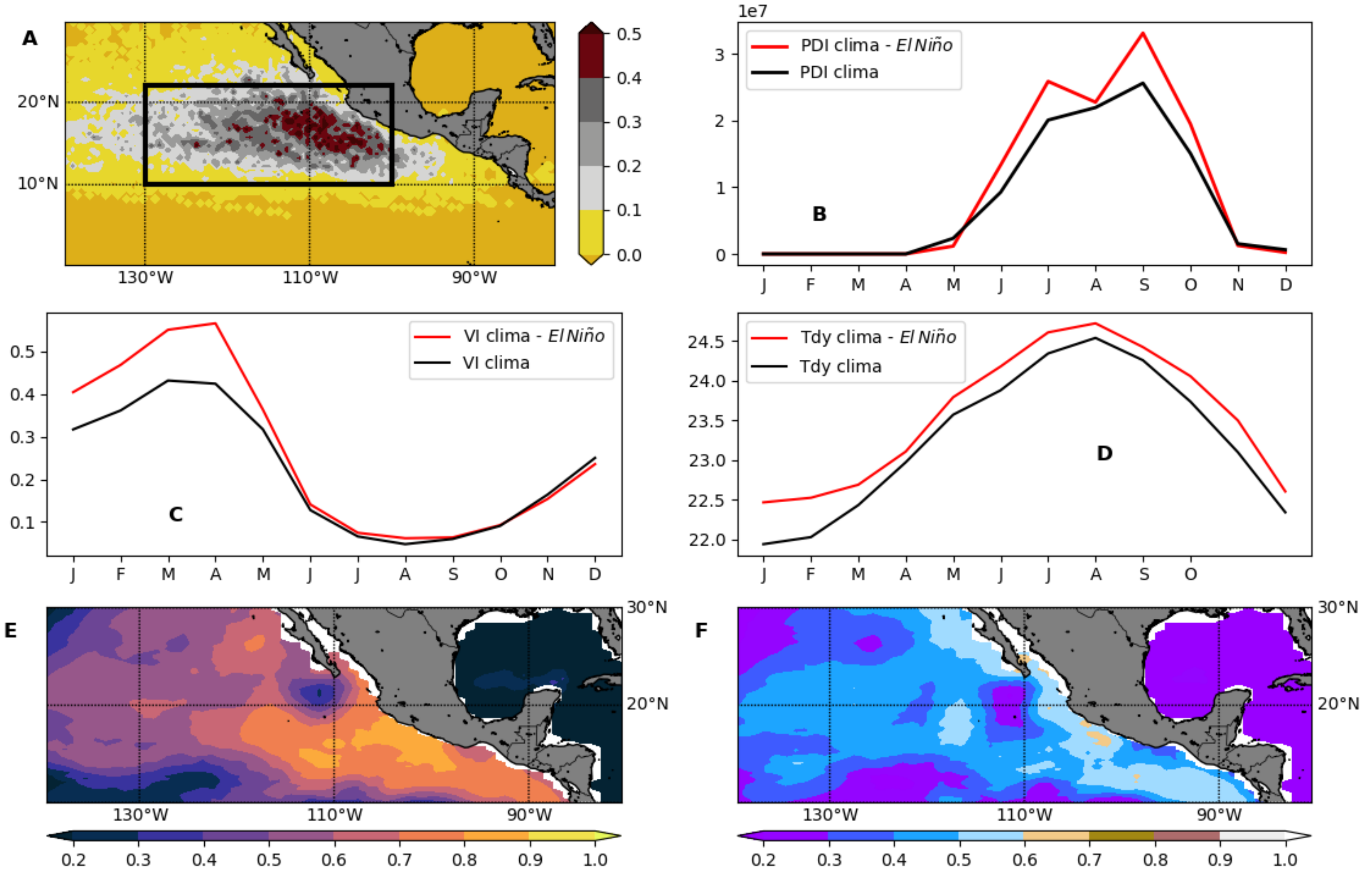

Figure 1. A) Track density, defined as the average number of storm locations per season, of Eastern Pacific hurricanes based on 40-years of data. The black rectangle represents approximately the region with highest track density. Climatological seasonal cycles of B) PDI (kt^3), C) VI and D) Tdy (°C) for all (black) and El Niño (red) years. El Niño years are defined as those years during which the previous December-February averaged ELI exceeds 161°E. VI and Tdy are averaged over the rectangular box shown in panel A. VI is calculated based on ERA5 reanalysis, while Tdy is based on NCEP-GODAS ocean reanalysis. E) First EOF of July-October averaged Tdy, expressed as the correlation between the leading PC time series and the time series of Tdy values at each grid point. F) Correlation between PDI and July-October averaged Tdy.

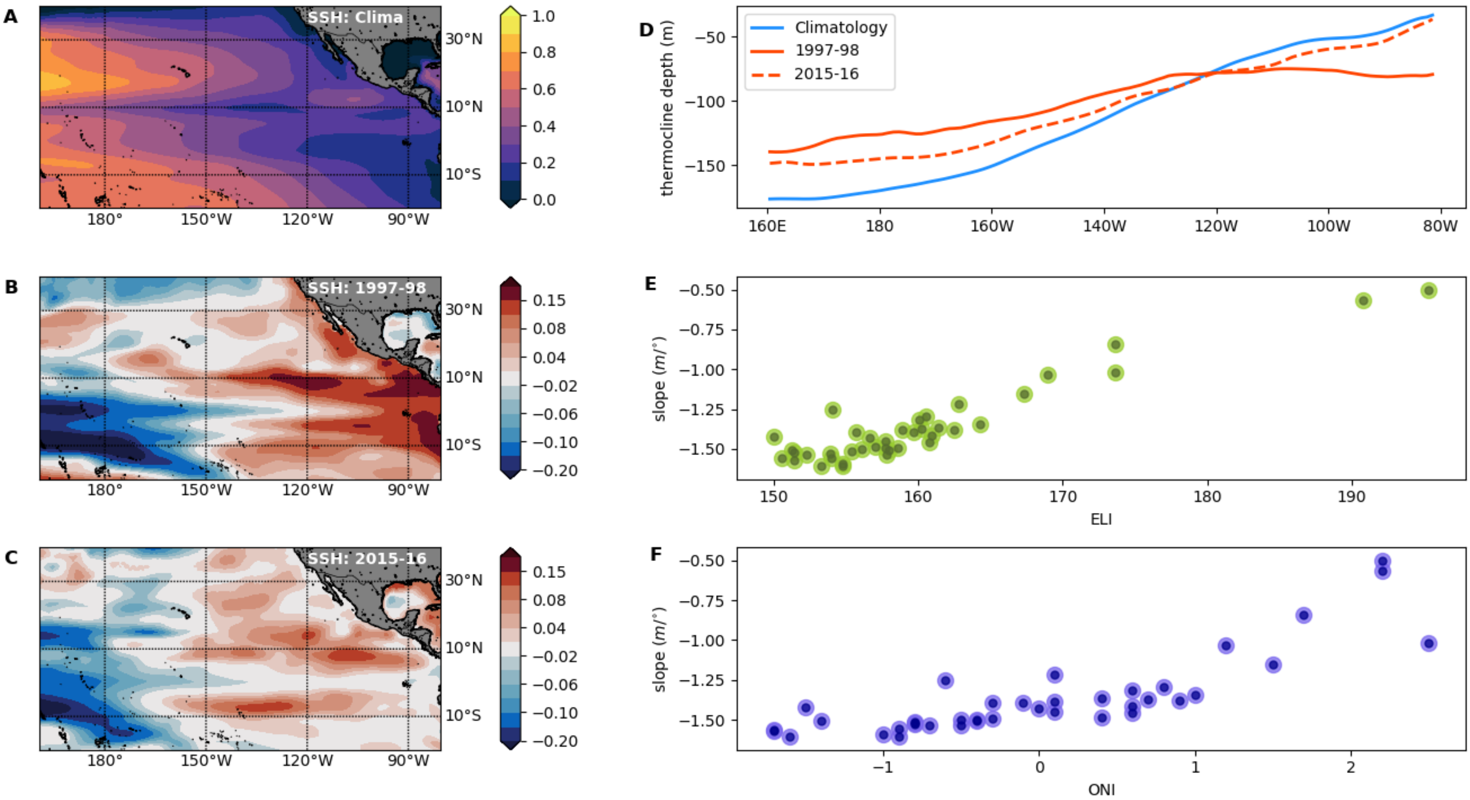

Figure 2. A) Climatological January-May averaged SSH (m). Anomalous January-May averaged SSH (m) following the B) 1997-98 El Niño and C) 2015-16 El Niño events. D) Thermocline depth (m), averaged over the months of January-May and, between 5°S and 5°N, from climatology (blue), following the 1997-98 El Niño (solid red) and following the 2015-16 El Niño (dashed red). Scatter between the slope of the January-May averaged thermocline depth and the previous December-February averaged E) ELI and F) ONI. Slope is evaluated between the date line and 80°W longitude.

Table 1. Correlation between various ENSO indices and PDI, Major Hurricane frequency (MH), frequency of Rapid Intensification (RI), and the first principal component timeseries for Tdy and TCHP. In the first three rows, the values outside the parenthesis are when the entire Eastern Pacific basin is considered (east of 140°W), and the values within the parenthesis are for the eastern part of the basin (east of 115°W). The underlined values are significant at the 90% level, while the values that are underlined and in bold are significant at the 95% level. Tdy and TCHP are based on NCEP-GODAS.

	ONI	SOI	MEI	ELI
PDI	0.16 (0.17)	<u>-0.23</u> (<u>-0.24</u>)	<u>0.20</u> (<u>0.23</u>)	<u>**0.28**</u>(<u>**0.34**</u>)
MH	0.15 (0.10)	-0.19 (-0.17)	0.19 (0.15)	<u>0.26</u> (<u>0.25</u>)
RI	0.13 (0.14)	-0.17 (-0.18)	0.15 (0.19)	<u>0.22</u> (<u>**0.30**</u>)
Tdy	<u>0.25</u>	<u>-0.25</u>	<u>0.24</u>	<u>**0.32**</u>
TCHP	0.17	-0.12	0.13	<u>0.20</u>

Acknowledgments

K.B., S.M.H. and L.R.L. acknowledge support from the Regional and Global Modeling and Analysis Program of the U.S. Department of Energy, Office of Science, Office of Biological and Environmental Research (BER). This research was also supported as part of the E3SM project, funded by BER. The Pacific Northwest National Laboratory is operated for DOE by Battelle Memorial Institute under contract DE-AC05-76RL01830. C.M.P. acknowledges support from the U.S. Department of Energy, Office of Science, Office of Biological and Environmental Research, Climate and Environmental Sciences Division, Regional and Global Model Analysis Program, under Award Number DE-AC02-05CH11231. The data for various analysis performed in this study are freely available for download from the various links provided in section 2.1.

References

Balaguru, K., Foltz, G. R., Leung, L. R., Asaro, E. D., Emanuel, K. A., Liu, H., & Zedler, S. E. (2015). Dynamic potential intensity: An improved representation of the ocean's impact on tropical cyclones. *Geophysical Research Letters*, *42*(16), 6739–6746.

Balaguru, K., Leung, L. R., & Yoon, J.-h. (2013). Oceanic control of northeast pacific hurricane activity at interannual timescales. *Environmental Research Letters*, *8*(4), 044009.

Balmaseda, M. A., Mogensen, K., & Weaver, A. T. (2013). Evaluation of the ecmwf ocean reanalysis system oras4. *Quarterly Journal of the Royal Meteorological Society*, *139*(674), 1132–1161.

Behringer, D., & Xue, Y. (2004). Evaluation of the global ocean data assimilation system at ncep: The pacific ocean. In *Proc. eighth symp. on integrated observing and assimilation systems for atmosphere, oceans, and land surface.*

Blake, E. S. (2009). Tropical cyclones of the eastern north pacific basin, 1949-2006.

Boucharel, J., Jin, F.-F., England, M. H., Dewitte, B., Lin, I., Huang, H.-C., & Balmaseda, M. A. (2016). Influence of oceanic intraseasonal kelvin waves on eastern pacific hurricane activity. *Journal of Climate*, *29*(22), 7941–7955.

Boucharel, J., Jin, F.-F., Lin, I., Huang, H.-C., & England, M. H. (2016). Different controls of tropical cyclone activity in the eastern pacific for two types of el niño. *Geophysical Research Letters*, *43*(4), 1679–1686.

Bryan, G. H. (2008). On the computation of pseudoadiabatic entropy and equivalent potential temperature. *Monthly Weather Review*, *136*(12), 5239–5245.

Cai, W., Borlace, S., Lengaigne, M., Van Rensch, P., Collins, M., Vecchi, G., ... others (2014). Increasing frequency of extreme el niño events due to greenhouse warming. *Nature climate change*, *4*(2), 111–116.

Camargo, S. J., Camp, J., Elsberry, R. L., Gregory, P. A., Klotzbach, P. J., Schreck III, C. J., ... others (2019). Tropical cyclone prediction on subseasonal time-scales. *Tropical Cyclone Research and Review*, *8*(3), 150–165.

Camargo, S. J., Robertson, A. W., Barnston, A. G., & Ghil, M. (2008). Clustering of eastern north pacific tropical cyclone tracks: Enso and mjo effects. *Geochemistry, Geophysics, Geosystems*, *9*(6).

Caron, L.-P., Boudreault, M., & Camargo, S. J. (2015). On the variability and predictability of eastern pacific tropical cyclone activity. *Journal of Climate*, *28*(24), 9678–9696.

Chiu, A. N. (1983). *Hurricane iwa, hawaii, november 23, 1982.* National Academies.

Chu, P.-S. (2004). *Enso and tropical cyclone activity.* Columbia University Press New York.

Coffman, M., & Noy, I. (2012). Hurricane iniki: measuring the long-term economic impact of a natural disaster using synthetic control. *Environment and Development Economics*, *17*(2), 187–205.

Collins, J. M., Klotzbach, P. J., Maue, R. N., Roache, D. R., Blake, E. S., Paxton, C. H., & Mehta, C. A. (2016). The record-breaking 2015 hurricane season in the eastern north pacific: An analysis of environmental conditions. *Geophysical Research Letters*, *43*(17), 9217–9224.

Collins, J. M., & Mason, I. (2000). Local environmental conditions related to seasonal tropical cyclone activity in the northeast pacific basin. *Geophysical research letters*, *27*(23), 3881–3884.

Corbosiero, K. L., Dickinson, M. J., & Bosart, L. F. (2009). The contribution of eastern north pacific tropical cyclones to the rainfall climatology of the southwest united states. *Monthly Weather Review*, *137*(8), 2415–2435.

Dawson, A. (2016). eofs: A library for eof analysis of meteorological, oceanographic, and climate data. *Journal of Open Research Software*, *4*(1).

DeMaria, M. (1996). The effect of vertical shear on tropical cyclone intensity change. *Journal of the atmospheric sciences*, *53*(14), 2076–2088.

Emanuel, K. (2005). Increasing destructiveness of tropical cyclones over the past 30 years. *Nature*, *436*(7051), 686–688.

Emanuel, K. A. (1999). Thermodynamic control of hurricane intensity. *Nature*, *401*(6754), 665–669.

Foltz, G. R., & Balaguru, K. (2016). Prolonged el niño conditions in 2014–2015 and the rapid intensification of hurricane patricia in the eastern pacific. *Geophysical Research Letters*, *43*(19), 10–347.

Fu, D., Chang, P., & Patricola, C. M. (2017). Intrabasin variability of east pacific tropical cyclones during enso regulated by central american gap winds. *Scientific reports*, *7*(1), 1–8.

Gray, W. M., & Brody, L. (1967). *Global view of the origin of tropical disturbances and storms.* Citeseer.

Gray, W. M., & Sheaffer, J. (1991). *El niño and qbo influences on tropical cyclone activity.* Cambridge University Press Cambridge.

Hersbach, H., & Dee, D. (2016). Era5 reanalysis is in production. *ECMWF newsletter*, *147*(7), 5–6.

Jáuregui, E. (2003). Climatology of landfalling hurricanes and tropical storms in mexico. *Atmósfera*, *16*(4), 193–204.

Jien, J. Y., Gough, W. A., & Butler, K. (2015). The influence of el niño–southern oscillation on tropical cyclone activity in the eastern north pacific basin. *Journal of climate*, *28*(6), 2459–2474.

Jin, F.-F. (1996). Tropical ocean-atmosphere interaction, the pacific cold tongue, and the el niño-southern oscillation. *Science*, *274*(5284), 76–78.
Jin, F.-F. (1997). An equatorial ocean recharge paradigm for enso. part i: Conceptual model. *Journal of the atmospheric sciences*, *54*(7), 811–829.
Jin, F.-F., Boucharel, J., & Lin, I.-I. (2014). Eastern pacific tropical cyclones intensified by el niño delivery of subsurface ocean heat. *Nature*, *516*(7529), 82–85.
Kanamitsu, M., Ebisuzaki, W., Woollen, J., Yang, S.-K., Hnilo, J., Fiorino, M., & Potter, G. (2002). Ncep–doe amip-ii reanalysis (r-2). *Bulletin of the American Meteorological Society*, *83*(11), 1631–1644.
Kaplan, J., Rozoff, C. M., DeMaria, M., Sampson, C. R., Kossin, J. P., Velden, C. S., ... others (2015). Evaluating environmental impacts on tropical cyclone rapid intensification predictability utilizing statistical models. *Weather and Forecasting*, *30*(5), 1374–1396.
Kessler, W. S., & McPhaden, M. J. (1995). Oceanic equatorial waves and the 1991–93 el nino. *Journal of Climate*, *8*(7), 1757–1774.
Kiladis, G. N., & van Loon, H. (1988). The southern oscillation. part vii: Meteorological anomalies over the indian and pacific sectors associated with the extremes of the oscillation. *Monthly weather review*, *116*(1), 120–136.
Kimberlain, T., Blake, E. S., & Cangialosi, J. P. (2016). Hurricane patricia (ep202015). *National Hurricane Center tropical cyclone report*.
Kimberlain, T. B. (2014). The 2013 eastern north pacific hurricane season: Mexico takes the brunt. *Weatherwise*, *67*(3), 35–42.
Klotzbach, P. J., & Blake, E. S. (2013). North-central pacific tropical cyclones: impacts of el niño–southern oscillation and the madden–julian oscillation. *Journal of climate*, *26*(19), 7720–7733.
Landsea, C. W., & Franklin, J. L. (2013). Atlantic hurricane database uncertainty and presentation of a new database format. *Monthly Weather Review*, *141*(10), 3576–3592.
Latif, M., & Keenlyside, N. S. (2009). El niño/southern oscillation response to global warming. *Proceedings of the National Academy of Sciences*, *106*(49), 20578–20583.
Maloney, E. D., & Hartmann, D. L. (2000). Modulation of eastern north pacific hurricanes by the madden–julian oscillation. *Journal of climate*, *13*(9), 1451–1460.
McPhaden, M. J. (1999). Genesis and evolution of the 1997-98 el niño. *Science*, *283*(5404), 950–954.
McPhaden, M. J., & Yu, X. (1999). Equatorial waves and the 1997–98 el niño. *Geophysical Research Letters*, *26*(19), 2961–2964.
Meinen, C. S., & McPhaden, M. J. (2000). Observations of warm water volume changes in the equatorial pacific and their relationship to el niño and la niña. *Journal of Climate*, *13*(20), 3551–3559.
Patricola, C. M., Chang, P., & Saravanan, R. (2016). Degree of simulated suppression of atlantic tropical cyclones modulated by flavour of el niño. *Nature Geosci*, *9*, 155–160.
Rappaport, E. N., Franklin, J. L., Avila, L. A., Baig, S. R., Beven, J. L., Blake, E. S., ... others (2009). Advances and challenges at the national hurricane center. *Weather and Forecasting*, *24*(2), 395–419.
Rayner, N., Parker, D. E., Horton, E., Folland, C. K., Alexander, L. V., Rowell, D., ... Kaplan, A. (2003). Global analyses of sea surface temperature, sea ice, and night marine air temperature since the late nineteenth century. *Journal of Geophysical Research: Atmospheres*, *108*(D14).
Ritchie, E. A., Wood, K. M., Gutzler, D. S., & White, S. R. (2011). The influence of eastern pacific tropical cyclone remnants on the southwestern united states. *Monthly Weather Review*, *139*(1), 192–210.
Rogers, R. F., Aberson, S., Bell, M. M., Cecil, D. J., Doyle, J. D., Kimberlain, T. B.,

... Velden, C. (2017). Rewriting the tropical record books: The extraordinary intensification of hurricane patricia (2015). *Bulletin of the American Meteorological Society*, *98*(10), 2091–2112.

Rolinski, T., Capps, S. B., Fovell, R. G., Cao, Y., D'Agostino, B. J., & Vanderburg, S. (2016). The santa ana wildfire threat index: methodology and operational implementation. *Weather and Forecasting*, *31*(6), 1881–1897.

Romero-Vadillo, E., Zaytsev, O., & Morales-Pérez, R. (2007). Tropical cyclone statistics in the northeastern pacific. *Atmósfera*, *20*(2), 197–213.

Shay, L. K., & Brewster, J. K. (2010). Oceanic heat content variability in the eastern pacific ocean for hurricane intensity forecasting. *Monthly Weather Review*, *138*(6), 2110–2131.

Tang, B., & Emanuel, K. (2012). A ventilation index for tropical cyclones. *Bulletin of the American Meteorological Society*, *93*(12), 1901–1912.

Trenberth, K. E. (1997). The definition of el nino. *Bulletin of the American Meteorological Society*, *78*(12), 2771–2778.

Wang, C., & Fiedler, P. C. (2006). Enso variability and the eastern tropical pacific: A review. *Progress in Oceanography*, *69*(2-4), 239–266.

Whitney, L. D., & Hobgood, J. S. (1997). The relationship between sea surface temperatures and maximum intensities of tropical cyclones in the eastern north pacific ocean. *Journal of Climate*, *10*(11), 2921–2930.

Williams, I. N., & Patricola, C. M. (2018). Diversity of enso events unified by convective threshold sea surface temperature: a nonlinear enso index. *Geophysical Research Letters*, *45*(17), 9236–9244.

Wolter, K., & Timlin, M. S. (2011). El niño/southern oscillation behaviour since 1871 as diagnosed in an extended multivariate enso index (mei. ext). *International Journal of Climatology*, *31*(7), 1074–1087.

Wyrtki, K. (1985). Water displacements in the pacific and the genesis of el niño cycles. *Journal of Geophysical Research: Oceans*, *90*(C4), 7129–7132.